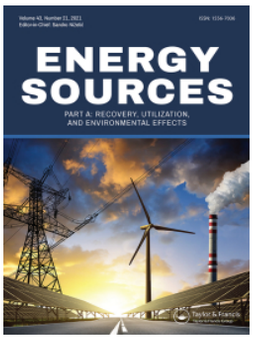

Taylor & Francis
Taylor & Francis Group

Energy Sources, Part A: Recovery, Utilization, and Environmental Effects

ISSN: (Print) (Online) Journal homepage: https://www.tandfonline.com/loi/ueso20

Biowaste-derived oxygen-self-doped three-dimensional interconnected porous carbon for electrochemical supercapacitor applications

Bidayatul Armynah, Erwinda Erwinda, Agustino Agustino, Erman Taer, Syahir Mahmud & Dahlang Tahir

To cite this article: Bidayatul Armynah, Erwinda Erwinda, Agustino Agustino, Erman Taer, Syahir Mahmud & Dahlang Tahir (2023) Biowaste-derived oxygen-self-doped three-dimensional interconnected porous carbon for electrochemical supercapacitor applications, Energy Sources, Part A: Recovery, Utilization, and Environmental Effects, 45:2, 6331-6342, DOI: 10.1080/15567036.2023.2215198

To link to this article: https://doi.org/10.1080/15567036.2023.2215198

Published online: 18 May 2023.

ENERGY SOURCES, PART A: RECOVERY, UTILIZATION, AND ENVIRONMENTAL EFFECTS
2023, VOL. 45, NO. 2, 6331–6342
https://doi.org/10.1080/15567036.2023.2215198

Taylor & Francis
Taylor & Francis Group

Biowaste-derived oxygen-self-doped three-dimensional interconnected porous carbon for electrochemical supercapacitor applications

Bidayatul Armynah[a], Erwinda Erwinda[a], Agustino Agustino[b], Erman Taer[b], Syahir Mahmud[c], and Dahlang Tahir[a]

[a]Department of Physics, Hasanuddin University, Makassar, Indonesia; [b]Department of Physics, Universitas Riau, Pekanbaru, Indonesia; [c]Department of Electrical Engineering, Universitas Atmajaya Makassar, Makassar, Indonesia

ABSTRACT

Biowaste for producing a biomaterial is an inexpensive, profuse, widely available, and viable natural source and has been extensively investigated and applied in a wide range of research fields. In this work, jackfruit leaf waste as a biowaste source was utilized to prepare a three-dimensional (3D) interconnected porous carbon framework self-doped with oxygen by KOH impregnation, carbonization, and activation under a CO_2 atmosphere. The as-prepared porous carbon has a 3D interconnected porous framework with a rich oxygen content of 36.82%, and high BET surface area of 455.687 $m^2\ g^{-1}$ with a pore volume of 0.522 $cm^3\ g^{-1}$. The 3D interconnected porous framework exhibits a high specific capacitance of 199 F g^{-1} with a maximum energy density of 27.64 Wh kg^{-1} at a power density of 99.60 W kg^{-1} at a sweep rate of 1 mV s^{-1} in a two-electrode setup. The correlation between structure and great performance of electrode materials is deeply studied. The great capacitive performance of porous carbon materials can be assigned to its 3D interconnected porous framework, high specific surface area, suitable pore size distributions, and advantageous heteroatom-doping, resulting in the rapid ion diffusion and sufficient charge storage along with the contributed pseudocapacitance behavior. Hence, the exciting results reveal an efficient, cost-effective, time-saving, and facile method to prepare 3D interconnected porous carbon frameworks self-doped with oxygen derived from natural biowaste sources for developing supercapacitor devices.

ARTICLE HISTORY
Received 9 February 2023
Revised 12 May 2023
Accepted 13 May 2023

KEYWORDS
Biowaste; Jackfruit leaf waste; 3D interconnected porous carbon framework; oxygen-self-doped; supercapacitor

Introduction

The rapid economic growth around the world worsens the energy crisis; thus, it is significant to expand green, sustainable, efficient, and environmentally amiable energy storage systems (ESSs). As one of the ESSs, supercapacitors (SCs) have fascinated tremendous attention due to their benefits such as high power density (Hor and Hashmi 2020; Liang, Liu, and Qi 2022), long lifetime cycle (Dai et al. 2020; Wang et al. 2020), low maintenance cost (Ali et al. 2021; Ma et al. 2019), and wide operating temperature range (Yanilmaz et al. 2019). The capacitive performance of a supercapacitor depends on electrodes, type of electrolyte, and type of device configuration. Several electrode materials such as porous activated carbon (Alcaraz et al. 2020; Rajesh et al. 2020), metal oxide (Khot and Kiani 2022; Racik et al. 2020), and carbon/polymer (Pourjavadi et al. 2018) have been synthesized to fabricate SC electrodes. Among them, porous activated carbon is the material of choice for SCs owing to its high surface, excellent physical and chemical stability, highly porous structure, and good electrical conductivity.

CONTACT Bidayatul Armynah armynah63@gmail.com; Dahlang Tahir dtahir@fmipa.unhas.ac.id Department of Physics, Hasanuddin University, Makassar 90245, Indonesia

Recently, biowaste-derived porous carbon for SC fabrication has garnered attention from researchers owing to its highly porous network, high surface area, renewability, abundance, and cost-effectiveness. Various biowaste sources such as cotton waste (Liu et al. 2023), tea seed meal (You et al. 2023), rice husk (Liu et al. 2022), *Zizania latifolia* (Zhao et al. 2022), *Tectona grandis* leaf (Taer et al. 2021), *lycium chinensis* (Xu et al. 2021), poplar catkin (Yang et al. 2021), pineapple leaf (Agustino et al. 2020), foxtail grass seeds (Liang, Liu, and Wu 2021), and so on have been studied and utilized for SC electrodes. However, porous carbon has lower specific capacitance and energy density compared to graphene and carbon nanotubes due to its poor electrical conductivity and disarranged and cramped porous structure (Panja, Bhattacharjya, and Yu 2015). To address this problem, designing porous carbon with excellent capacitive performance is urgently needed. Currently, various methods, including increasing porosity and heteroatom doping, to enhance the chemical surface structure and increase electron distribution have been used to further enhance the capacitive performance of SC electrode materials (Z. Liu et al. 2020; Xu et al. 2022). Moreover, heteroatom doping is another impressive route to improve the performance of porous carbon and provides a combination of electric double-layer capacitance (EDLC) and pseudocapacitance behaviors. In addition to producing a definite pseudocapacitance effect, heteroatoms can enhance the wettability and polarity of the electrode material surface, thus boosting the capacitive performance of the electrode materials (Liu et al. 2022; You et al. 2023). Heteroatom doping can be categorized into two strategies: (i) self-doping can be prepared via direct carbonization of biowaste sources to perform hetero atom doping, and (ii) external doping involves multiple steps that are tedious, complicated, and long-time processes.

In this work, a 3D interconnected porous carbon framework self-doped with oxygen was prepared from jackfruit leaf waste by KOH impregnation, carbonization, and activation under a CO_2 atmosphere. The main objective of this work was to prepare a 3D interconnected porous carbon framework self-doped with oxygen via the efficient, cost-effective, time-saving, and facile method. Afterward, the framework was applied as electrode material for SC devices.

The preparation process of the porous carbon framework did not include an external dopant such as urea, thiourea, melamine, phosphoric acid, and amines become as novelty of this work. In comparison with some reported references using external dopant such as urea (Ma et al. 2017), melamine (Miao et al. 2022), phosphoric acid (Li et al. 2022), ammonia (Kolanowski et al. 2022), boric acid (Sun, Xu, and Wang 2022), and so on. However, none of these studies analyzed the 3D interconnected porous framework based on jackfruit leaf waste as a porous carbon source. Thus, compared with external doping, self-doping is a more cost-effective, facile, and green process. The as-prepared porous carbon material has a high specific surface area of 455.687 $m^2\ g^{-1}$, 3D interconnected porous framework, and pore size in the micropore range. These physical characteristics have resulted in a high specific capacitance of 199 F g^{-1} in a symmetrical two-electrode setup. Thus, the jackfruit leaf waste can be an alternative porous carbon source for synthesizing oxygen-self-doped activated carbon as an electrode material for SC devices.

Experimental methods

Jackfruit leaf porous-activated carbon (JLPAC) preparation

Jackfruit leaf waste was collected from Tamalanrea Regency, South Sulawesi, Indonesia. The leaf waste was dried under direct sunlight for 2 days. Afterward, the leaf was cut into small pieces and dried in an electric oven at 110 °C for 2 h. The dried leaf was precarbonized at 250 °C for 2.5 h to remove water molecules to obtain self-adhesive properties on the samples. The precarbonized sample was ground to fine particles of fewer than 53 microns. Fine particles (50 g) were impregnated into 0.3 mol L^{-1} KOH solution and were stirred in a hot plate at 80 °C for 2 h. The reaction of carbon precursors against KOH is provided by the following equation: $6KOH + 2C \rightarrow 2K + 3H_2 + 2K_2CO_3$ (Lillo-Ródenas et al. 2004; Lillo-Ródenas, Cazorla-Amorós, and Linares-Solano 2003). This is a solid/liquid redox reaction with the main products being potassium (K), hydrogen (H_2), and potassium carbonate (K_2CO_3). The

as-activated samples were dried for 3 × 24 h at 110 °C. After that, under a pressure of 8 metric tons, the as-activated samples were molded into a coin-like shape using a hydraulic press. Then, the samples were carbonized at different temperatures, that is, 500°C, 600°C, and 700 °C, followed by activation at 850 °C for an hour under a CO_2 atmosphere. The as-obtained samples were immersed in distilled water until neutral pH and were labeled as JLPAC-500, JLPAC-600, and JLPAC-700. The schematic diagram for the preparation of porous carbon is provided in Figure 1.

Physical parameter characterizations

Various techniques were used to evaluate the physical characteristics of the as-prepared JLPAC. Microstructures and elemental composition were inspected by SEM-EDX, JEOL-JSM 6510 LA. Purity and crystal phase were characterized by X-ray diffractometers with CuKα (l = 0.154 nm) in the range of 20°-80°. Adsorption/desorption isotherms of N_2 were collected using Quantachrome Instruments Nova version 10.01 to investigate the porous characteristics of the JLPACs. Before physisorption measurements at 77.3 K, the samples were degassed at 120 °C for 4 hrs in a vacuum. Specific surface area (SSA) was measured by the Brunauer–Emmett–Teller (BET) equation. The t-plot theory was employed to obtain the micropore surface area and pore volume. Barrett–Joyner–Halenda (BJH) method was applied to calculate pore size distributions.

Self-standing electrode preparation

The electrodes were prepared using a self-standing model without any adhesive material, polymer pigment, and carbon black. First, two pieces of electrodes for each variation were polished until a thickness of 0.2 mm, diameter of 0.8 cm, and mass loading of ±0.008 g cm^{-2}. Then, the two pieces of electrodes were assembled into a coin-like structure with a duck eggshell membrane as the separator. H_2SO_4 (1 mol L^{-1}) and stainless steel plate type 316 L were used as the electrolyte and current collector. Finally, the electrodes and duck eggshell membrane were soaked in a 1 mol L^{-1} H_2SO_4 electrolyte before use.

Electrochemical measurement

The electrochemical performance of the self-standing JLPAC electrodes was measured by cyclic voltammetry (CV) tests in a symmetrical two-electrode setup. These measurements were operated in the voltage range of 0–1 V with sweep rates 1–10 mV s^{-1} at room temperature. The specific capacitance (C_s) and areal capacitance (C_A) of the JLPACs based on the CV test were determined using the following formula:

$$C_s = \frac{4I}{s \times m} \tag{1}$$

$$C_A = M \times C_s \tag{2}$$

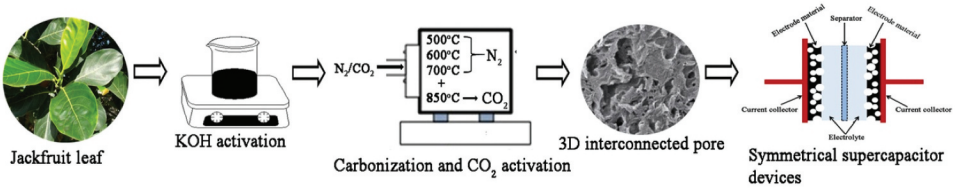

Figure 1. Schematic diagram for the preparation of porous carbon.

where I (A), s (mV s^{-1}), m (g), and M (g cm^{-2}) are the charge/discharge current, sweep rates, total mass of both electrodes, and electrode mass loading, respectively. The energy and power densities of the self-standing JLPAC electrodes were determined using equations (3) and (4):

$$E_d = \frac{C_s(\Delta V^2)}{2 \times 3.6} \tag{3}$$

$$P_d = 3600 \times \frac{E_d}{\Delta t} \tag{4}$$

where E_d (Wh kg^{-1}), P_d (W kg^{-1}), and Δt (s) is energy density, power density, and discharge time, respectively.

Results and discussion

Physical parameter analysis

The microstructures of JLPAC-600 and JLPAC-700 based on SEM images at different magnifications can be seen in Figure 2. Figure 2 (a-b) shows the surface structure of JLPAC-600. Its surface has a 3D interconnected porous framework with numerous micro-mesopores. The structure contains abundant porous networks as a result of KOH impregnation in the raw materials. Figure 2 (c-d) depicts the surface structure of JLPAC-700. The figures show that, after increasing the carbonization temperature from 600 to 700°C and activating at 850°C, its surface structure remains as a 3D bonded pore framework. However, the 3D pores on the surface tend to be fewer than those on the surface of JLPAC-600. 3D porous networks have greater advantages over 2D networks for ESSs, owing to their large contact areas, numerous active sites, and structural stability (Liang et al. 2020). In addition, the

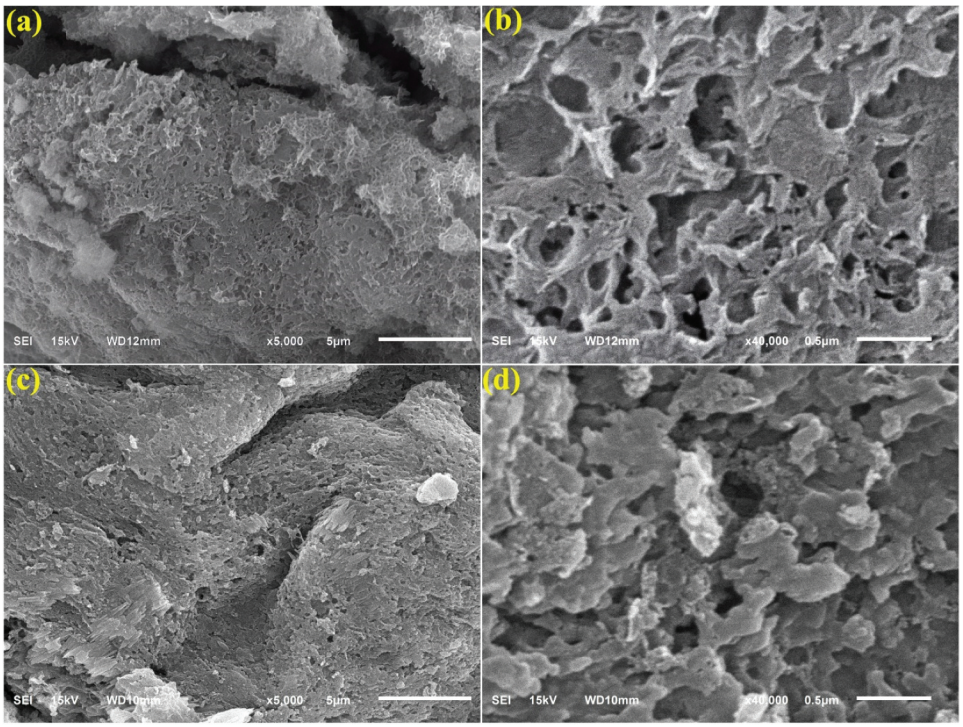

Figure 2. SEM photomicrograph of JLPAC-600 at 5000× (a), JLPAC-600 at 40,000× (b), JLPAC-700 at 5000× (c), and JLPAC-700 at 40,000× (d).

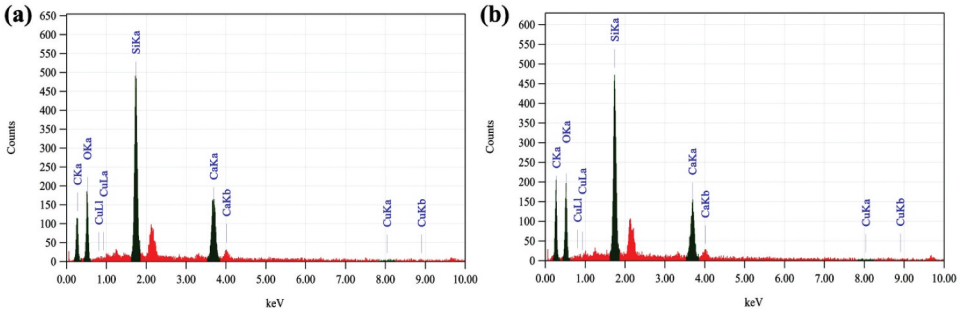

Figure 3. EDS spectra of JLPAC-600 (a) and JLPAC-700 (b).

interconnected porous structure in the JLPAC sample is helpful in the transfer of ions in electrochemical reactions.

The EDX spectra of the JLPAC-600 and JLPAC-700 are shown in Figure 3. From Figure 3, if the carbonization temperature is increased, the carbon content of the sample increases, and the oxygen content decreases. As seen in Figure 2(a) and (b), JLPAC-600 and JLPAC-700 have carbon contents of 47.10% and the highest 54.96%, respectively. The as-prepared samples are also rich in oxygen content, with 36.82% for JLPAC-600 and 32.54% for JLPAC-700. JLPAC-600 contains oxygen and has an interconnected porous framework, thus facilitating effective ion diffusion, thereby improving hydrophilicity and wettability on electrode surfaces, generating the pseudocapacitance effect (He et al. 2021; Jia et al. 2022), thereby enhancing the capacitive performance of JLPAC-600. The complete chemical compositions of JLPAC-600 and JLPAC-700 are listed in Table 1.

Figure 4 (a – b) depicts the XRD spectra of JLPAC-600 and JLPAC-700. Both samples show similar XRD spectra including the peak positions at different intensities for both peaks. JLPAC-600 and JLPAC-700 show two characteristic peaks at 22°-24° and 42°-44°, assigned to the (002) and (100) crystal planes, related to the graphite structure and amorphous carbon framework, respectively. Sharp peaks at 29.77°, 37.79°, 44.03°, and 64.39° are found in the JLPAC-600 spectrum, while those at 29.69°, 37.76°, 44.03°, and 64.41°are found in the JLPAC-700 spectrum. These peaks correspond to the

Table 1. Elemental composition of the JLPACs.

	Elemental composition				
Samples	C (%)	O (%)	Si (%)	Ca (%)	Cu (%)
JLPAC-600	47.10	36.82	10.29	5.75	0.04
JLPAC-700	54.96	32.54	8.30	4.21	-

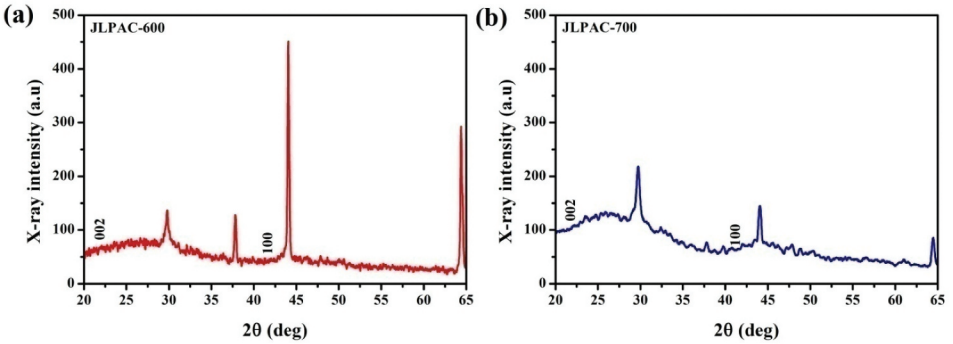

Figure 4. XRD spectra of JLPAC-600 (a) and JLPAC-700 (b).

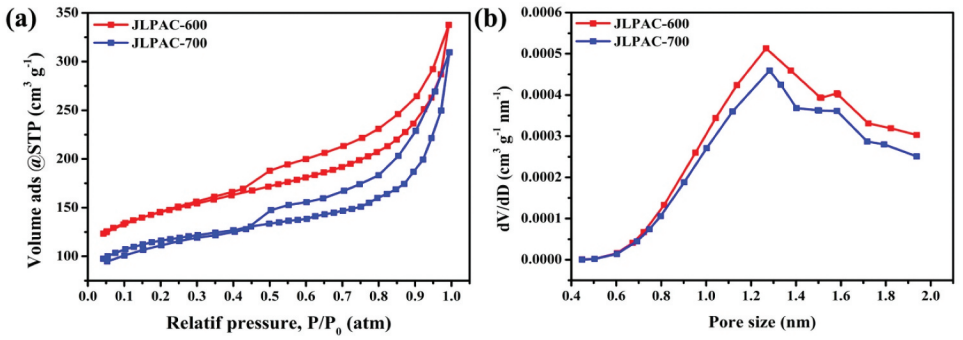

Figure 5. (a) Adsorption/desorption isotherms of N_2 and (b) pore size distributions of the JLPAC samples.

Table 2. Porous characteristics of the JLPACs.

Samples	S_{BET} ($m^2\ g^{-1}$)	S_{micro} ($m^2\ g^{-1}$)	S_{meso} ($m^2\ g^{-1}$)	V_{micro} ($cm^3\ g^{-1}$)	V_{tot} ($cm^3\ g^{-1}$)	D_{pore} (nm)
JLPAC-600	455.687	141.870	313.817	0.081	0.522	4.59
JLPAC-700	356.991	81.310	275.681	0.046	0.479	5.37

crystalline features of SiO_2, MgO, $CaCO_3$, and CaO according to the JCPDS card nos. 89–1668, 89–7746, 82–1690, and 82–1691, respectively.

Adsorption/desorption isotherms of N_2 were used to analyze the SSA and pore characteristics of JLPAC-600 and JLPAC-700. As shown in Figure 5(a), JLPAC-600 and JLPAC-700 display type IV isotherms with H3-type hysteresis loop at P/P_0 >0.4 atm, which is revealing of the existence of mesoporosity (Liang et al. 2019; S. Ma et al. 2019) and pore slit-like shape (Sui et al. 2014; Surya and Michael 2020). When the relative pressure (P/P_0) approaches 1, N_2 adsorption is significantly larger, suggesting the presence of macropores (Guo et al. 2021). JLPAC-600 and JLPAC-700 have BET surface areas (S_{BET}) of 455.687 and 356.991 $m^2\ g^{-1}$, respectively. This value is higher than those of 3D porous carbon from *Moringa oleifera* leaves (412.196 $m^2\ g^{-1}$) (Taslim, Apriwandi, and Taer 2022) and activated carbon from palm petiole (436 $m^2\ g^{-1}$) (Kanjana et al. 2021). Furthermore, JLPAC-600 and JLPAC-700 have pore volumes of 0.522 and 0.479 $cm^3\ g^{-1}$, respectively.

The pore size distributions in the micropore range of JLPAC-600 and JLPAC-700 are illustrated in Figure 5(b). Both samples contain various types of pores with sizes of 0.44–1.94 nm, in agreement with the SEM results. It is shown that JLPAC-600 has a 3D interconnected porous framework, which is advantageous to enhance the capacitive performance of electrodes. It is believed that micropores can serve as absorption sites for EDLC, the mesopores serve as diffusion promoters, and the macropores serve as the storage areas of electrolyte (Lin et al. 2019). Moreover, the ultra-micropores in both samples, which are about less than 0.7 nm in diameter, can be made the dissolved ions closer to the carbon walls (by distorted solvation, the electric double-layer is closer to the electrode materials, which increases capacitance) in the electrolytes (Shao et al. 2020). As a result, JLPAC-600 has the capability to provide excellent capacitive performance because of its large SSA and appropriate pore size distributions. The completely porous characteristics of JLPAC-600 and JLPAC-700 are summarized in Table 2.

Electrochemical behavior analysis

As discussed in the previous sections, the physical parameters of the JLPAC samples play a crucial role in improving the electrochemical accessibility of the electrode material for charge storage (Scheers, Fantini, and Johansson 2014). To confirm the electrochemical behavior of the self-standing JLPAC samples carbonized at different temperatures, CV was employed using a symmetrical two-electrode

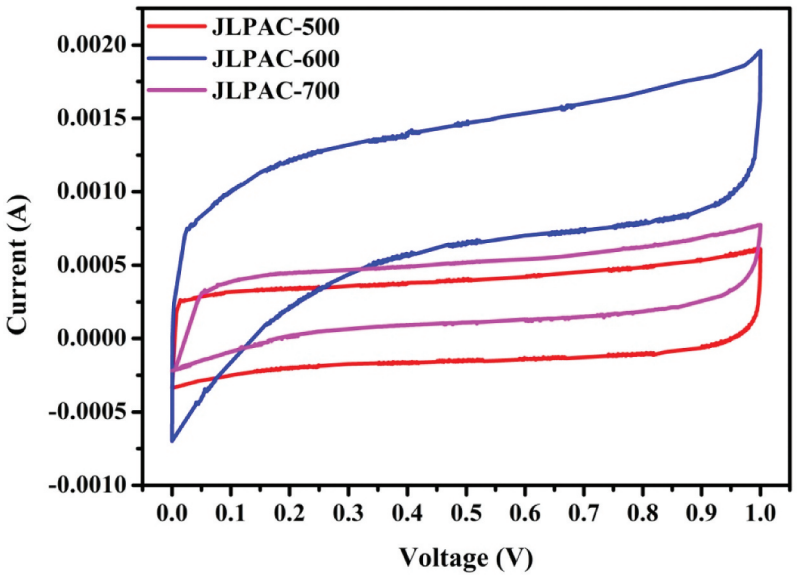

Figure 6. CV plots of JLPAC samples at sweep rate of 1 mV s^{-1}.

setup with a 1 mol L^{-1} H_2SO_4 electrolyte, and the results are displayed in Figure 6 (a). All the CV plots of JLPAC-500, JLPAC-600, and JLPAC-700 at a sweep rate of 1 mV s^{-1} present quasi-rectangular shapes, demonstrating that the JLPACs have an ideal electric double-layer formation. Among them, the JLPAC-600 electrode has excellent performance, as shown by the highest enclosed area, indicating the largest capacitance value, also in agreement with the SEM-EDS, surface area, and pore size analyses. The specific capacitances of JLPAC-500, JLPAC-600, and JLPAC-700 are 161, 199, and 109 F g^{-1}, respectively. Meanwhile, the calculated areal capacitance of JLPAC electrodes is 1.56 F cm^{-2}, 1.04 F cm^{-2}, and 0.77 F cm^{-2}, respectively. These results demonstrate that JLPAC-600 exceeds storage capacity and its value is higher than those of JLPAC-500 and JLPAC-700. The high specific and areal capacitances may be attributed to the 3D interconnected porous framework of the electrode material, which provides a short and direct path for ion diffusion into electrode pores (Shan et al. 2016; Wang et al. 2022). In addition, the chemical composition effect observed for JLPAC-600 by physical parameter analysis seems to be favorable for assisting diffusion of SO_4^{2-} ions and interface chemical reactions, leading to higher specific capacitance. For JLPAC-600, having various pore size distributions has proven more effective for storing and releasing ions during the electrochemical process. In addition, JLPAC-600 having a higher SSA and pore volume serves as a supporting porous material that provides active sites and transports ions to facilitate electrochemical reactions.

Figure 7(a–c) presented the CV plots of JLPAC electrodes at different sweep rates. Generally, all the CV plots of the JLPAC-500, JLPAC-600, and JLPAC700 electrodes at different sweep rates of 1, 2, and 5 mV s^{-1} have still retained its quasi-rectangular shapes, indicating the electrical double-layer behavior for porous carbon based on biowaste materials. However, the CV plot of JLPAC-600 at sweep rates of 2 and 5 mV s^{-1} (see Figure 7b) shows a quasi-rectangular shape with an obvious hump at a voltage range of 0.01–0.25 V, indicating that JLPAC-600 has a combination of electric double-layer and pseudocapacitance behavior. This behavior can be ascribed to the existence of a high oxygen amount in JLPAC-600, as shown in the EDX analysis, leading to a significant pseudocapacitive behavior contribution. Meanwhile, the CV plots of JLPAC-500 and JLPAC-700 (see Figure 7(a and c)) did not show the existence of a hump at a certain voltage range, indicating that electric double-layer behavior dominates in both samples. Figure 7(d) shows the specific capacitances as a function of sweep rates. The specific capacitance of JLPAC-600 declines with a raising sweep rate because of the diffusion time limitation of the electrolyte ions and vice versa. Further, at

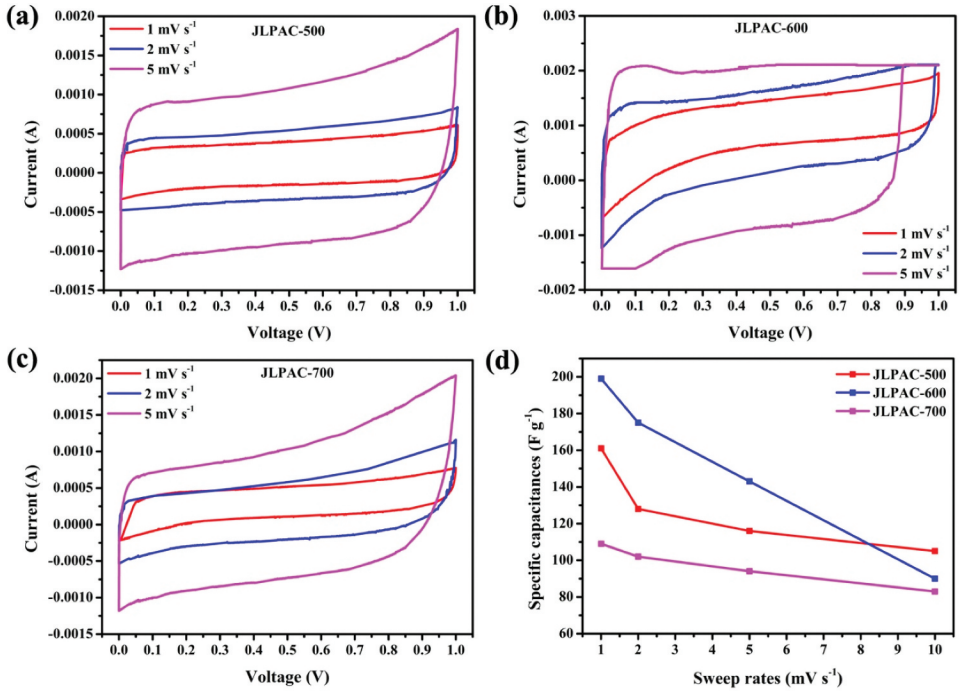

Figure 7. CV plots at various sweep rates of JLPAC-500 (a), JLPAC-600 (b), JLPAC-700 (c), and (d) specific capacitances vs. sweep rates.

Table 3. The specific capacitance of the JLPACs at different sweep rates.

	Specific capacitance (F g^{-1})			
Samples	1 mV s^{-1}	2 mV s^{-1}	5 mV s^{-1}	10 mV s^{-1}
JLPAC-500	161	128	116	105
JLPAC-600	199	175	143	90
JLPAC-700	109	102	94	83

a low sweep rate, the specific capacitances of the JLPACs are larger owing to the involvement of micropores, which contribute to the charge of the double-layer capacitive system. Meanwhile, at a high sweep rate, mesopores and micropores become more pronounced and accessible for efficient charging. In all these contexts, the quasi-rectangular shapes are found without any change because of the interconnected porous framework, which indicates rapid ion diffusion even at a high sweep rate (Iozzo et al. 2015; Simon and Gogotsi 2008). The specific capacitances of the JLPACs at various sweep rates are listed in Table 3. When the sweep rate is 1 mV s^{-1}, the specific capacitances of JLPAC-500, JLPAC-600, and JLPAC-700 are 161 F g^{-1}, 199 F g^{-1}, and 109 F g^{-1}, respectively. When the sweep rate is raised to 10 mV s^{-1}, the capacitance retentions of JLPAC-500, JLPAC-600, and JLPAC-700 are 34.7%%, 54.8%%, and 23.8%, respectively.

Another parameter like power densities and energy is crucial to evaluate the performance of supercapacitors. From the formulas (3) and (4), the energy density of the JLPAC-500, JLPAC-600, and JLPAC-700 are 22.36, 27.64, 15.14 Wh kg^{-1} with corresponding power densities of at 80.58, 99.60, and 54.56 W kg^{-1}, respectively. The calculated energy densities of the JLPAC samples are comparable to the values reported previously for porous carbon-based supercapacitors with heteroatom-doping and are summarized in Table 4. Generally, the synergistic effects of the 3D interconnected porous framework, rich in oxygen content, high surface area, and advantageous heteroatom-doping provide an excellent capacitive performance of the porous carbon materials derived from jackfruit leaf.

Table 4. The capacitive performance of JLPACs compared to other biowaste derived from heteroatom-doped activated carbon.

Precursor	Dopants	S_{BET} ($m^2\ g^{-1}$)	C_s (F g^{-1})	E_d (Wh kg^{-1})	P_d (W kg^{-1})	References
Juncus	N-doped	1379.9	205	28.6	502.5	(He et al. 2020)
Cicada slough	N-O-codoped	2086	290	9.8	62.2	(Y. Liu et al. 2020)
Lotus leaves	O, N, S, self-doped	3601	294	-	-	(Liu et al. 2020)
Chitin	N, O heteroatoms-doped	1488	69.6	9.67	-	(Y. Wang et al. 2020)
Sorghum seeds	N, O-codoped	2132	279.3	13.8	298	(Feng et al. 2021)
Allium cepa peel	O self-doped	2962	189.4	22.1	39.6	(Ali et al. 2021)
Black fungus	O, N-codoped	1227.3	209.3	7.3	-	(Zhong et al. 2021)
Cotton fabric	O, N, P and S heteroatoms-doped	643.7	140.5	28.4	120	(Sun et al. 2021)
Euphorbia milii	N, S, P self-doped	2349	290.3	39.75	496.5	(Nanda and Badhulika 2022)
Turtle shells	O and N self-doped	2828	100.1	45.1	450	(Chen et al. 2022)
Cotton seed meal	Heteroatom self-doped	2361	71.8	10	125	(Jia et al. 2022)
Shrimp shell waste	N self-doped	1508	163	11.23	248.8	(Nanda et al. 2022)
Chitosan and graphene oxide	N, O heteroatoms-doped	984	58.7	14.7	-	(Mo et al. 2022)
Jackfruit leaf waste	O self-doped	455.687	199	27.64	99.60	This work

Conclusion

The findings demonstrate that the oxygen-self-doped 3D interconnected porous carbon framework derived from jackfruit leaf waste prepared by KOH impregnation, carbonization at different temperatures, and activation under a CO_2 atmosphere and successfully applied as an electrode material in SC devices with conclusion as follows:

- The samples were doped without the addition of external-doping agents such as urea, thiourea, and melamine, which means that green process.
- The 3D interconnected porous framework, rich oxygen content, high surface area, and advantageous heteroatom-doping, the porous carbon materials exhibit a rapid ion diffusion, enough charge storage, and contribute to pseudo capacitance behavior.
- JLPAC-600 and JLPAC-700 show diffraction peaks at 22°–24° and 42°–44° for (002) and (100) crystal planes indicating graphite structure and amorphous carbon, respectively.
- The JLPAC-600 electrode demonstrates an excellent electrochemical performance with a specific capacitance as high as 199 F g^{-1} and delivered maximum energy density 27.64 Wh kg^{-1}, which is of good competition with various reported porous carbon materials.
- This work shows efficient, cost-effective, time-saving, and facile method for preparing an oxygen-self-doped 3D interconnected porous carbon framework from a natural biowaste source reveals potential for developing porous carbon-based SC devices.

Acknowledgements

The authors are grateful to the faculty of mathematics and natural sciences, Hasanuddin University for the financial support through the research grants faculty of mathematics and natural sciences, Hasanuddin University.

Disclosure statement

No potential conflict of interest was reported by the authors.

Notes on contributors

Dr. Bidayatul Armynah is a scientist/ senior lecturer and head of physics master degree study program at Hasanuddin University.

Ms. Erwinda Erwinda is an project fellow at Energy for Environment at Hasanuddin University

Mr, Agustino Agustino is an project fellow at energy for environment at Riau University.

Prof. Erman Taer is a senior professor at Riau university, He was appointed as a Professor in Material Physics especially for supercapacitor.

Mr. Syahir Mahmud is a senior lecturer for electrical engineering at Aniversitas Atmajaya Makassar.

Prof. Dahlang Tahir is as a Professor in Material Physics in 2014. His research activities included nanocomposite material for food packaging (bioplastics), for medical physics (phantom and shielding), and for environment (Energy, photocatalyst and adsorbent heavy metals). He is currently director of publication management centre at UNHAS.

ORCID

Agustino Agustino http://orcid.org/0000-0002-3669-1064
Dahlang Tahir http://orcid.org/0000-0002-8241-3604

References

Agustino, A., A. Taslim, R. Amri, E. Taer, and E. Taer. 2020. The physical and electrochemical properties of activated carbon electrode derived from pineapple leaf waste for supercapacitor applications. *Journal of Physics Conference Series* 1655 (1):012008-012008–7. doi:10.1088/1742-6596/1655/1/012008.

Alcaraz, L., A. Adán-Más, P. Arévalo-Cid, M. D. F. Montemor, and F. A. López. 2020. Activated carbons from winemaking biowastes for electrochemical double-layer capacitors preparation of the activated carbons from. *Frontiers in Chemistry* 8 (August):1–10. doi:10.3389/fchem.2020.00686.

Ali, G. A. M., S. Supriya, K. F. Chong, E. R. Shaaban, H. Algarni, T. Maiyalagan, and G. Hegde. 2021. Superior supercapacitance behavior of oxygen self-doped carbon nanospheres: A conversion of Allium cepa peel to energy storage system. *Biomass Conversion and Biorefinery* 11 (4):1311–23. doi:10.1007/s13399-019-00520-3.

Chen, H., X. Lei, T. Yu, X. Guan, and H. Yuan. 2022. Ultra-high specific capacitance of self-doped 3D hierarchical porous turtle shell-derived activated carbon for high-performance supercapacitors. *Ceramics International* 48 (4):5289–98. doi:10.1016/j.ceramint.2021.11.072.

Dai, Z., P. G. Ren, W. He, X. Hou, F. Ren, Q. Zhang, and Y. L. Jin. 2020. Boosting the electrochemical performance of nitrogen-oxygen co-doped carbon nanofibers based supercapacitors through esterification of lignin precursor. *Renewable Energy* 162:613–23. doi:10.1016/j.renene.2020.07.152.

Feng, T., S. Wang, Y. Hua, P. Zhou, G. Liu, K. Ji, Z. Lin, S. Shi, X. Jiang, and R. Zhang. 2021. Synthesis of biomass-derived N,O-codoped hierarchical porous carbon with large surface area for high-performance supercapacitor. *Journal of Energy Storage* 44 (PA):103286. doi:10.1016/j.est.2021.103286.

Guo, Y., T. Wang, D. Wu, and Y. Tan. 2021. One-step synthesis of in-situ N, S self-doped carbon nanosheets with hierarchical porous structure for high performance supercapacitor and oxygen reduction reaction electrocatalyst. *Electrochimica acta* 366:137404. doi:10.1016/j.electacta.2020.137404.

He, W., P. Ren, Z. Dai, X. Hou, F. Ren, and Y. Jin. 2021. Hierarchical porous carbon composite constructed with 1-D CNT and 2-D GNS anchored on 3-D carbon skeleton from spent coffee grounds for supercapacitor. *Applied Surface Science* 558 (April):149899. doi:10.1016/j.apsusc.2021.149899.

He, G., G. Yan, Y. Song, L. Wang, and L. Wang. 2020. Biomass juncus derived nitrogen-doped porous carbon materials for supercapacitor and oxygen reduction reaction. *Frontiers in Chemistry* 8 (April):1–10. doi:10.3389/fchem.2020.00226.

Hor, A. A., and S. A. Hashmi. 2020. Optimization of hierarchical porous carbon derived from a biomass pollen-cone as high-performance electrodes for supercapacitors. *Electrochimica acta* 356:136826. doi:10.1016/j.electacta.2020.136826.

Iozzo, D. A. B., M. Tong, G. Wu, and E. P. Furlani. 2015. Numerical analysis of electric double layer capacitors with mesoporous electrodes: effects of electrode and electrolyte properties. *The Journal of Physical Chemistry C* 119 (45):25235–42. doi:10.1021/acs.jpcc.5b08409.

Jia, B., Q. Mian, D. Wu, and T. Wang. 2022. Heteroatoms self-doped porous carbon from cottonseed meal using K2CO3 as activator and DES electrolyte for supercapacitor with high energy density. *Materials Today Chemistry* 24:100828. doi:10.1016/j.mtchem.2022.100828.

Kanjana, K., P. Harding, T. Kwamman, W. Kingkam, and T. Chutimasakul. 2021. Biomass-derived activated carbons with extremely narrow pore size distribution via eco-friendly synthesis for supercapacitor application. *Biomass & bioenergy* 153 (August):106206. doi:10.1016/j.biombioe.2021.106206.

Khot, M., and A. Kiani. 2022. Synthesis of self-grown nanostructured NiO via pulse ionization for binderless psuedo-capacitor electrode. *Journal of Energy Storage* 55 (PD):105779. doi:10.1016/j.est.2022.105779.

Kolanowski, Ł., M. Graś-Ligocka, P. Krawczyk, T. Buchwald, K. Lota, and G. Lota. 2022. Ozonation with ammoxidation as a method of obtaining O, N-doped carbon electrode material to electrochemical capacitors. *Electrochimica acta* 413 (February):1–7. doi:10.1016/j.electacta.2022.140130.

Liang, Y., X. Liu, and X. Qi. 2022. Hierarchical nanoarchitectonics of ordered mesoporous carbon from lignin for high-performance supercapacitors. *International Journal of Biological Macromolecules* 213 (38):610–20. doi:10.1016/j.ijbiomac.2022.06.005.

Liang, X., R. Liu, and X. Wu. 2021. Biomass waste derived functionalized hierarchical porous carbon with high gravimetric and volumetric capacitances for supercapacitors. *Microporous and Mesoporous Materials* 310 (June 2020):110659. doi:10.1016/j.micromeso.2020.110659.

Liang, Y., Y. Lu, G. Xiao, J. Zhang, H. Chi, and Y. Dong. 2020. Hierarchical porous nitrogen-doped carbon microspheres after thermal rearrangement as high performance electrode materials for supercapacitors. *Applied Surface Science* 529:147141. doi:10.1016/j.apsusc.2020.147141.

Liang, J., Z. Xiao, Y. Gao, X. Xu, D. Kong, M. Wagner, and L. Zhi. 2019. Ionothermal strategy towards template-free hierarchical porous carbons for supercapacitive energy storage. *Carbon* 143:487–93. doi:10.1016/j.carbon.2018.11.065.

Li, D., Y. Guo, Y. Li, Z. Liu, and Z. Chen. 2022. Waste-biomass tar functionalized carbon spheres with N/P Co-doping and hierarchical pores as sustainable low-cost energy storage materials. *Renewable Energy* 188:61–69. doi:10.1016/j.renene.2022.01.109.

Lillo-Ródenas, M. A., D. Cazorla-Amorós, and A. Linares-Solano. 2003. Understanding chemical reactions between carbons and NaOH and KOH: An insight into the chemical activation mechanism. *Carbon* 41 (2):267–75. doi:10.1016/S0008-6223(02)00279-8.

Lillo-Ródenas, M. A., J. Juan-Juan, D. Cazorla-Amorós, and A. Linares-Solano. 2004. About reactions occurring during chemical activation with hydroxides. *Carbon* 42 (7):1371–75. doi:10.1016/j.carbon.2004.01.008.

Lin, Y., Z. Chen, C. Yu, and W. Zhong. 2019. Heteroatom-doped sheet-like and hierarchical porous carbon based on natural biomass small molecule peach gum for high- performance supercapacitors. *ACS Sustainable Chemistry & Engineering* 7 (3):3389–403. doi:10.1021/acssuschemeng.8b05593.

Liu, H., R. Liu, C. Xu, Y. Ren, D. Tang, C. Zhang, F. Li, X. Wei, and R. Zhang. 2020. Oxygen–nitrogen–sulfur self-doping hierarchical porous carbon derived from lotus leaves for high-performance supercapacitor electrodes. *Journal of Power Sources* 479 (May):228799. doi:10.1016/j.jpowsour.2020.228799.

Liu, Y., H. Tan, Z. Tan, and X. Cheng. 2022. Rice husk derived capacitive carbon prepared by one-step molten salt carbonization for supercapacitors. *Journal of Energy Storage* 55 (PA):105437. doi:10.1016/j.est.2022.105437.

Liu, D., G. Xu, X. Yuan, Y. Ding, and B. Fan. 2023. Pore size distribution modulation of waste cotton-derived carbon materials via citrate activator to boost supercapacitive performance. *Fuel* 332 (P1):126044. doi:10.1016/j.fuel.2022.126044.

Liu, Z., S. Zhang, L. Wang, T. Wei, Z. Qiu, and Z. Fan. 2020. High-efficiency utilization of carbon materials for supercapacitors. *Nano Select* 1 (2):244–62. doi:10.1002/nano.202000011.

Ma, F., S. Ding, H. Ren, and Y. Liu. 2019. Sakura-based activated carbon preparation and its performance in supercapacitor applications. *RSC Advances* 9 (5):2474–83. doi:10.1039/c8ra09685f.

Ma, G., W. Tang, K. Sun, Z. Zhang, E. Feng, and Z. Lei. 2017. Coprinus comatus-based nitrogen-doped active carbon for high performance supercapacitor. *Nano* 12 (8):1–15. doi:10.1142/S179329201750103X.

Miao, J., Z. Zhai, S. Wang, Y. Xu, S. Du, X. Wang, X. Dong, B. Ren, and Z. Liu. 2022. Facile synthesis of hierarchical porous two-dimensional N-doped carbon nanosheets as bi-functional electrode for superior supercapacitor and photo-catalyst. *Journal of Cleaner Production* 369 (August):133369. doi:10.1016/j.jclepro.2022.133369.

Mo, F., H. Zhang, Y. Wang, C. Chen, and X. Wu. 2022. Heteroatom-doped hierarchical porous carbon for high performance flexible all-solid-state symmetric supercapacitors. *Journal of Energy Storage* 49 (February):104122. doi:10.1016/j.est.2022.104122.

Nanda, O. P., and S. Badhulika. 2022. Biomass derived Nitrogen, Sulphur, and Phosphorus self-doped micro-meso porous carbon for high-energy symmetric supercapacitor – with a detailed study of the effect of different current collectors. *Journal of Energy Storage* 56 (October):106042. doi:10.1016/j.est.2022.106042.

Nanda, O. P., N. K. Das, P. Sekar, A. Ramadoss, and B. Saravanakumar. 2022. Bio-waste derived self-templated, nitrogen self-doped porous carbon for supercapacitors. *Bioresource Technology Reports* 19 (August):101198. doi:10.1016/j.biteb.2022.101198.

Panja, T., D. Bhattacharjya, and J. S. Yu. 2015. Nitrogen and phosphorus co-doped cubic ordered mesoporous carbon as a supercapacitor electrode material with extraordinary cyclic stability. *Journal of Materials Chemistry A* 3 (35):18001–09. doi:10.1039/c5ta04169d.

Pourjavadi, A., M. Doroudian, A. Ahadpour, and B. Pourbadiei. 2018. Preparation of flexible and free-standing graphene-based current collector via a new and facile self-assembly approach: Leading to a high performance porous graphene/polyaniline supercapacitor. *Energy* 152:178–89. doi:10.1016/j.energy.2018.03.138.

Racik, K. M., A. Manikandan, M. Mahendiran, P. Prabakaran, J. Madhavan, and M. V. Antony. 2020. Fabrication of manganese oxide decorated copper oxide (MnO 2/CuO) nanocomposite electrodes for energy storage supercapacitor devices. *Physica E Low-Dimensional Systems & Nanostructures* 119 (January):114033. doi:10.1016/j.physe.2020.114033.

Rajesh, M., R. Manikandan, S. Park, B. C. Kim, W. J. Cho, K. H. Yu, and C. J. Raj. 2020. Pinecone biomass-derived activated carbon: The potential electrode material for the development of symmetric and asymmetric supercapacitors. *International Journal of Energy Research* 44 (11):8591–605. doi:10.1002/er.5548.

Scheers, J., S. Fantini, and P. Johansson. 2014. A review of electrolytes for lithium-sulphur batteries. *Journal of Power Sources* 255:204–18. doi:10.1016/j.jpowsour.2014.01.023.

Shan, D., J. Yang, W. Liu, J. Yan, and Z. Fan. 2016. Biomass-derived three-dimensional honeycomb-like hierarchical structured carbon for ultrahigh energy density asymmetric supercapacitors. *Journal of Materials Chemistry A* 4 (35):13589–602. doi:10.1039/c6ta05406d.

Shao, H., Y. Wu, Z. Lin, P. Simon, and P. Simon. 2020. Nanoporous carbon for electrochemical capacitive energy storage. *Chemical So* 49 (10):3005–39. doi:10.1039/d0cs00059k.

Simon, P., and Y. Gogotsi. 2008. Materials for electrochemical capacitors. *Nature Materials* 7 (11):845–54.

Sui, Z. Y., Q. H. Meng, J. T. Li, J. H. Zhu, Y. Cui, and B. H. Han. 2014. High surface area porous carbons produced by steam activation of graphene aerogels. *Journal of Materials Chemistry A* 2 (25):9891–98. doi:10.1039/c4ta01387e.

Sun, C., Z. Guo, M. Zhou, X. Li, Z. Cai, and F. Ge. 2021. Heteroatoms-doped porous carbon electrodes with three-dimensional self-supporting structure derived from cotton fabric for high-performance wearable supercapacitors. *Journal of Power Sources* 482 (May 2020):228934. doi:10.1016/j.jpowsour.2020.228934.

Sun, Y., D. Xu, and S. Wang. 2022. Self-assembly of biomass derivatives into multiple heteroatom-doped 3D-interconnected porous carbon for advanced supercapacitors. *Carbon* 199 (August):258–67. doi:10.1016/j.carbon.2022.08.026.

Surya, K., and M. S. Michael. 2020. Novel interconnected hierarchical porous carbon electrodes derived from bio-waste of corn husk for supercapacitor applications. *Journal of Electroanalytical Chemistry* 878:114674. doi:10.1016/j.jelechem.2020.114674.

Taer, E., M. Melisa, A. Agustino, R. Taslim, W. Sinta, and A. Apriwandi. 2021. Biomass-based activated carbon monolith from Tectona grandis leaf as supercapacitor electrode materials. *Energy Sources, Part A: Recovery, Utilization, & Environmental Effects* 00 (00):1–12. doi:10.1080/15567036.2021.1950871.

Taslim, R., A. Apriwandi, and E. Taer. 2022. Novel moringa oleifera leaves 3D porous carbon-based electrode material as a high-performance EDLC supercapacitor. *ACS Omega* 7:36489–502. doi:10.1021/acsomega.2c04301.

Wang, T., X. He, W. Gong, Z. Kou, Y. Yao, S. Fulbright, K. F. Reardon, and M. Fan (2022). Three-dimensional, heteroatom-enriched, porous carbon nanofiber flexible paper for free-standing supercapacitor electrode materials derived from microalgae oil. *Fuel Processing Technology*, *225*(July 2021), 107055. 10.1016/j.fuproc.2021.107055

Wang, J., X. Zhang, Z. Li, Y. Ma, and L. Ma. 2020. Recent progress of biomass-derived carbon materials for supercapacitors. *Journal of Power Sources* 451 (October 2019):227794. doi:10.1016/j.jpowsour.2020.227794.

Xu, P., J. Tong, L. Zhang, Y. Yang, X. Chen, J. Wang, and S. Zhang. 2022. Dung beetle forewing-derived nitrogen and oxygen self-doped porous carbon for high performance solid-state supercapacitors. *Journal of Alloys and Compounds* 892:162129. doi:10.1016/j.jallcom.2021.162129.

Xu, H., Y. Zhang, L. Wang, Y. Chen, and S. Gao. 2021. Hierarchical porous biomass-derived carbon framework with ultrahigh surface area for outstanding capacitance supercapacitor. *Renewable Energy* 179:1826–35. doi:10.1016/j.renene.2021.08.008.

Yang, J., K. X. Liu, Q. Y. Liu, and X. C. Zheng. 2021. Biomass waste-derived mesopore-dominant porous carbon for high-efficiency capacitive energy storage. *Journal of Alloys and Compounds* 885:161218. doi:10.1016/j.jallcom.2021.161218.

Yanilmaz, M., M. Dirican, A. M. Asiri, and X. Zhang. 2019. Flexible polyaniline-carbon nanofiber supercapacitor electrodes. *Journal of Energy Storage* 24:100766. doi:10.1016/j.est.2019.100766.

You, Z., L. Zhao, K. Zhao, H. Liao, S. Wen, Y. Xiao, B. Cheng, and S. Lei. 2023. Highly tunable three-dimensional porous carbon produced from tea seed meal crop by-products for high performance supercapacitors. *Applied Surface Science* 607 (June 2022):155080. doi:10.1016/j.apsusc.2022.155080.

Zhao, K., L. Zhao, W. Zhou, L. Rao, S. Wen, Y. Xiao, B. Cheng, and S. Lei. 2022. Pore regulation of well-developed honeycomb-like carbon materials from Zizania latifolia for supercapacitors. *Journal of Energy Storage* 52 (PB):104910. doi:10.1016/j.est.2022.104910.

Zhong, X., Q. Mao, Z. Li, Z. Wu, Y. Xie, S. H. Li, G. Liang, and H. Wang. 2021. Biomass-derived O, N-codoped hierarchically porous carbon prepared by black fungus andHericium erinaceusfor high performance supercapacitor. *RSC Advances* 11 (45):27860–67. doi:10.1039/d1ra03699h.